JOURNAL OF AGRICULTURAL AND FOOD CHEMISTRY

ARTICLE

pubs.acs.org/JAFC

Structure and Physical Properties of Starch/Poly Vinyl Alcohol/Sodium Montmorillonite Nanocomposite Films

Samer S. Ali, Xiaozhi Tang, Sajid Alavi,* and Jon Faubion

Department of Grain Science and Industry, Kansas State University, 201 Shellenberger Hall, Manhattan, Kansas 66506, United States

ABSTRACT: Nanocomposites of starch, poly vinyl alcohol (PVOH), and sodium montmorillonite (Na^+MMT) were produced by solution mixing and cast into films. Tensile strength (TS) and elongation at the break (E%) of the films ranged from 11.60 to 22.35 MPa and 28.93−211.40%, respectively, while water vapor permeability (WVP) ranged from 0.718 to 1.430 g·mm/kPa·h·m^2. In general, an increase in Na^+MMT content (0−20%) enhanced TS and decreased E% and WVP. Use of higher molecular weight PVOH increased both TS and E% and also decreased WVP. Mechanical properties were negatively affected, but water vapor barrier properties improved with increasing starch content (0−80%). X-ray diffraction and transmission electron microscopy were used to analyze the nanostructure, and molecular conformations and interactions in the multicomponent nanocomposites were inferred from glass transition behavior. Interactions between starch and PVOH were strongest, followed by polymer/clay interactions. On the basis of this insight, a conceptual model was presented to explain the phenomena of intercalation and exfoliation in the starch/PVOH/Na^+MMT nanocomposites.

KEYWORDS: nanocomposites, biodegradable, poly vinyl alcohol, starch, sodium montmorillonite

INTRODUCTION

Packaging plays a variety of important roles in the food industry. The major role of packaging is to protect food from spoilage by microbial contamination, physical damage, or biochemical reactions.[1−3] Packaging also provides ease in handling, storage efficiency, attractiveness, and product information for food.[1] The ideal food packaging material serves all of these purposes and is also cost efficient. Different types of materials, including plastics, cardboard, and metal, are used for food packaging depending on specific needs. The use of plastics in food packaging, including films, is common and increasing because of low cost and functional advantages over other materials.[1]

According to the Municipal Solid Waste report issued by the U.S. Environmental Protection Agency (EPA) for the year 2008, 76.76 million tons of waste was generated from packaging materials. This included 13.01 million tons from plastics with 4.89 million tons of plastic packaging in the form of films. Only 13.2% of this plastic packaging waste was recycled, while only 9.8% of plastic films were recovered; the rest was added to landfills. Recycling plastics is challenging because of their diverse nature. Plastics that are not recycled become a permanent part of our environment. Moreover, plastics are commonly produced from petroleum-based sources that are nonrenewable. According to the U.S. Energy Information Administration, 331 million barrels of liquid petroleum gases (LPG) and natural gas liquids (NGL) were used to make plastic materials and resins in 2006. This amounted to 4.6% of the total oil consumption in the U.S. An online report from Resource Conservation Manitoba stated that every year 100 billion plastic bags are used in the U.S., which takes 12 million barrels of oil, an amount that can produce 240 million gallons of gasoline.

Though plastics are one of the cheapest sources available for food packaging, their reliance on petroleum and their long-term impact on the environment have spurred research in recent years on alternative packaging based on renewable and biodegradable materials.[4] Starch is one such inexpensive, abundantly available, and renewable material that can be used for making biodegradable packaging films. Starch is composed of linear amylose (poly-α-1,4-D-glucopyranoside) and branched amylopectin (poly-α-1,4-D-glucopyranoside and poly-α-1,6-D-glucopyranoside)[5] (Figure 1a). Starch films are very brittle in nature (elongation ranging from 4 to 8%) and have poor water barrier properties (water vapor permeability ranging from 0.77 to 1.61 g·mm/kPa·hr·m^2).[6−8] In comparison, plastic films have high tensile strength (10−80 MPa) and elongation at the break (200−800%)[9] and low water vapor permeability (0.002−0.05 g·mm/kPa·h·m^2).[10] To improve the properties of starch-based films, researchers have blended starch with other polymers such as polyhydroxyalkanoates,[11] poly lactic acid (PLA)[12,13] and poly vinyl alcohol (PVOH).[14−17]

PVOH is produced by hydrolysis of poly vinyl acetate and contains secondary hydroxyl groups in every alternate carbon[18] (Figure 1b). PVOH can be used to make composites with starch because the two polymers are highly compatible and form hydrogen bonds easily.[19−21] Films from starch and PVOH blends not only show improved mechanical properties over starch alone[14,17] but also are biodegradable.[21] However, PVOH is a poor barrier for moisture, just like starch, and is also expensive. Higher starch content in starch/PVOH composite films would minimize the cost but at the same time lead to deterioration in mechanical properties.[15,22] Therefore, there is a clear need to further improve such composite films.

An innovative approach to improve the mechanical and barrier properties of polymer films is to produce nanocomposites by

Received: March 19, 2011
Accepted: September 20, 2011
Revised: September 18, 2011
Published: September 20, 2011

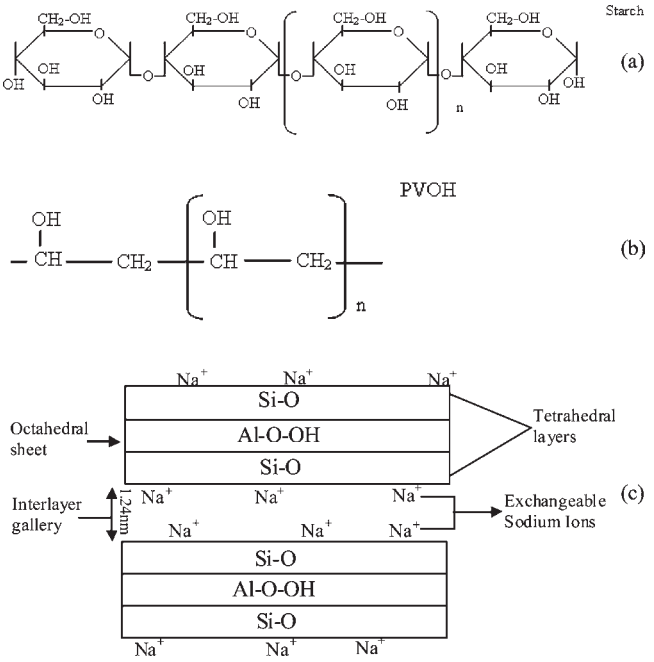

Figure 1. (a) Molecular structure of starch poly-α-1,4-D-glucopyranoside chain (present in both amylose and amylopectin); (b) molecular structure of PVOH; and (c) schematic for the molecular structure of Na^+MMT.

adding nanoscale particles. Clay minerals are a diverse class of layered silicates that have been used for producing nanocomposites with polymers,[4,23] and smectite clays are a subgroup commonly used in such nanocomposites due to their swelling properties and capacity to host water and organic molecules between their layers. These clays have high cation exchange capacity, large surface area, and high aspect ratio.[24] Montmorillonite (MMT) is a smectite clay that exists as platelets of two tetrahedral silicate layers with an inner (sandwiched) octahedral aluminum oxide sheet. Some of the aluminum atoms are replaced with magnesium creating a difference in valences and a negative charge distribution within the platelets. These charges are balanced by positively charged ions such as Na^+ (Figure 1c). Hydration of these sodium ions causes the clay to swell and provides the ability to host polymer chains between the layers, which is facilitated by attractive forces such as hydrogen bonds.[23] When Na^+MMT is mixed with a polymer, three distinct composite structures can form. If the polymer is not miscible with clay, it will stay in a separate phase, and no structural change will occur to the platelets. These types of composites are called microcomposites. If the polymer can enter clay interlayer regions without disrupting the layered structure, the resulting composites are called intercalated nanocomposites. The third type of composite structure corresponds to exfoliated nanocomposites, where clay with a disrupted layered structure is dispersed in the polymer matrix.[23,25] Starch is compatible with Na^+MMT due to the interaction between its polar hydroxyl groups and the Na^+ ions of nanoclay. This results in well intercalated or exfoliated nanocomposites, which help in improving the mechanical and barrier properties of starch films.[6−8,26,27] PVOH is also highly compatible with Na^+MMT, and films made from these nanocomposites exhibit better mechanical and barrier properties than films from PVOH alone.[19,28]

Table 1. PVOH Types Used for Studying Molecular Weight Effect

PVOH type	molecular weight[a]	viscosity (cps)
Celvol107	31,000−50,000	5.5−6.6
Celvol310	60,000−70,000	9−11
Celvol325	100,000−130,000	28−32
Celvol350	150,000−186,000	62−72

[a] Molecular weights were estimated from viscosity ranges given by the manufacturer.

On the basis of the above discussion, it is reasonable to expect that Na^+MMT is compatible with starch/PVOH composites as well and can form multicomponent nanocomposites with enhanced physical properties. Plasticizers can facilitate increased movement of PVOH and starch biopolymers into the interlayer galleries of Na^+MMT and lead to the formation of well intercalated and exfoliated systems. Glycerol is the conventional plasticizer used in starch/PVOH blends as it forms hydrogen bonds with both polymers, which replace the strong bonds between and within starch and PVOH.[20] Hydrogen bonding between glycerol and PVOH molecules also hinders the formation of crystallites in the plasticized films.[29]

Nanocomposites based on starch/PVOH/Na^+MMT have been studied recently.[5,19,30−32] However, little is still known about the various interactions that take place in such a multicomponent system. This study aims to bridge this gap by investigating molecular interactions in starch/PVOH/Na^+MMT nanocomposites and their impact on mechanical and barrier properties of films.

MATERIALS AND METHODS

Materials. Normal corn starch (Corn Products International, Westchester, IL) was the base material in all treatments. Four fully hydrolyzed brands of poly vinyl alcohol having different molecular weights (Table 1; Celvol107 < Celvol310 < Celvol325 < Celvol350) were obtained from Celanese Corporation (Dallas, TX). Other materials used in the synthesis of the nanocomposites included Na+MMT (Nanocor Inc., Arlington Heights, IL) and glycerol (The Chemistry Store.com, Cayce, SC).

Preparation of Nanocomposites and Film Casting. A solution was prepared by mixing 4 parts (by weight) starch/PVOH/Na+MMT/glycerol with 96 parts of water and then heating this mixture at 95 °C for 30 min with constant stirring. The proportions of starch, PVOH, and Na+MMT were varied depending on treatment, as described later. Glycerol was used as a plasticizer at a concentration of 30% (polymer basis) in all experiments. The heated solution was cooled to 55 °C, and equal amounts (60 g) were poured in 150 mm × 15 mm Petri dishes. The water was allowed to evaporate by drying for 24−36 h at room temperature, and the resulting films were peeled off and stored in airtight bags at room temperature for further tests.

Moisture Content. Moisture content of films was measured using the AACC 44-19.01 standard air-oven method (drying at 135 °C).

X-ray Diffraction. The dispersion of Na+MMT in nanocomposite films was studied using X-ray diffraction (XRD). The X-ray diffractometer (XRG 3100; Philips Electronics, Netherlands) was operated at 35 kV and 20 mA. Scans were carried out at diffraction angles (2θ) of 1.5−10.0° and a scan speed of 1°/min with a step size of 0.04°. X-ray radiation with a wavelength (λ) of 0.154 nm was generated from a Cu−Kα source. The interlayer spacing of Na+MMT or *d*-spacing was

estimated from XRD scans by using Bragg's Law as follows:

$$D = \frac{\lambda}{2 \sin \theta} \quad (1)$$

where, D = d-spacing (nm), λ = wavelength of X-ray beam (nm), and θ = the angle of incidence.

Transmission Electron Microscopy. The structure of nanocomposites and clay dispersion was visually observed using transmission electron microscopy (TEM). The electron microscope (CM100; Philips, Mahwah, NJ) was operated at 100 kV. The solution prepared for film casting was put on a carbon-coated copper grid and dried for one minute to make a film, which was then analyzed using TEM.

Thermal Analysis. Glass transition temperature (T_g), corresponding change in heat capacity (ΔC_p), and melting temperature (T_m) of nanocomposite films were measured using differential scanning calorimetry or DSC (Q100; TA Instruments, New Castle, DE). Films were conditioned at 23 °C and 50% RH for 3 days prior to testing. Samples (8−10 mg) were hermetically sealed in aluminum pans and heated from 10 to 250 °C at a rate of 10 °C/min. An empty aluminum pan was used as reference.

Tensile Properties. Tensile properties of films were measured with a texture analyzer (TA-XT2; Stable Micro Systems Ltd., UK) using the standard ASTM D882-02 method described previously.[6,7] Films were cut into 2 cm × 8 cm strips and were conditioned at 23 °C and 50% RH. Ends of the test specimen were mounted on grips 40 mm apart, and extension was carried out at a cross-head speed of 1 mm/s. Tensile strength (TS) and elongation at the break (E%) were calculated as follows:

$$\mathrm{TS} = \frac{L_p}{a} \times 10^{-6} \quad (2)$$

where TS = tensile strength (MPa), L_p = peak load (N), and a = cross-sectional area of samples (m^2).

$$\mathrm{E}\% = \frac{\Delta L}{L} \times 100 \quad (3)$$

where ΔL = increase in length at breaking point (mm), and L = original length (40 mm).

Water Vapor Permeability. Water vapor permeability was determined according to the standard ASTM E96-00 method described previously.[6,7] Films were tightly fixed with screws on top of aluminum test cells (area = 30 cm^2) containing a desiccant (silica gel). These test cells were placed in a relative humidity chamber at 25 °C and 75% relative humidity (RH), and were allowed to equilibrate for 2 h. Thereafter, weight of the test cells was recorded, and the measurement was repeated every 12 h over three days. The weight of the cells was plotted as a function of time for each sample, and the slope of the best-fit straight line ($\Delta G/\Delta t$) was used to calculate the water vapor transmission rate as follows:

$$\mathrm{WVTR} = \frac{\Delta G/\Delta t}{A} \quad (4)$$

where WVTR = water vapor transmission rate ($g/h \cdot m^2$), $\Delta G/\Delta t$ = rate of weight change (g/h), and A = test area (m^2). WVTR was then used to calculate the water vapor permeability as follows:

$$\mathrm{WVP} = \frac{\mathrm{WVTR} \times L}{\Delta P} \quad (5)$$

where WVP = water vapor permeability ($g \cdot mm/kPa \cdot h \cdot m^2$), L = film thickness (mm), and ΔP = partial pressure difference across the films (kPa). The film thickness was measured from five different locations for each film using a digital micrometer (Marathon Watch Company Ltd., Ontario, Canada), and the average thickness was used for all calculations.

Experimental Design and Statistical Analysis. Three sets of experiments were conducted for the preparation of the nanocomposite films. First, Na^+MMT contents of 0, 5, 10, 15, and 20% (polymer basis) were used while maintaining the same PVOH type (Celvol 325) and base polymer proportions (2:1 ratio of starch and PVOH). Second, PVOH of four different molecular weights were used at a constant base polymer proportion (1:1) and Na^+MMT concentration (10%). Third, the proportion of starch in the base polymer mix was varied (0, 20, 33, 50, 67, and 80%), while keeping Na^+MMT concentration (10%) and PVOH type (Celvol 325) constant. Thus, the experimental design comprised a total of 15 treatments, all of which were replicated three times. Data were analyzed using SAS statistical analysis software (Version 9; SAS Institute Inc. Cary, NC). Analysis of variance (ANOVA) was used to determine the effect of treatment, and statistical significance of differences in means was determined using the Tukey HSD multiple-comparison method at $p < 0.05$.

RESULTS AND DISCUSSION

Na^+MMT Content. The X-ray diffraction scan for natural Na^+MMT showed a peak angle of 7.11° with a corresponding d-spacing of 1.24 nm (Figure 2). Previous studies have reported similar 2θ and d-spacing for Na^+MMT.[6,7,33] XRD patterns of starch/PVOH (2:1) composite films with 0 to 20% MMT are also shown in Figure 2. As expected, no XRD peak was observed for starch/PVOH alone (0% Na^+MMT) due to the absence of clay and the amorphous nature of melted PVOH and starch.[6] An XRD peak was also absent at 5% Na^+MMT, while composites with 10% Na^+MMT had a low intensity broadened peak between 2θ of 3.5−5.0° (lower than the diffraction angle for Na^+MMT alone). This indicated that nanocomposites with highly or partially exfoliated structures were formed at Na^+MMT loading of 5% and 10%, respectively. XRD peaks of relatively higher intensity and narrower range were observed for 15 and 20% Na^+MMT, corresponding to 2θ of 4.30° and 6.58° and d-spacing of 2.06 and 1.34 nm, respectively. These peaks were also at a lower diffraction angle than pure Na^+MMT, which indicated the entrance of starch and PVOH polymers into the interlayer galleries, an increase in d-spacing between clay platelets, and the formation of nanocomposites with intercalated structure. These results also suggest that the degree of exfoliation/intercalation decreased with an increase in Na^+MMT content from 5 to 20%. The nanostructures revealed by transmission electron microscopy (Figure 3) corresponded to the inferences drawn from XRD analysis. TEM scans for nanocomposites with Na^+MMT levels of 5 and 10% confirmed full and partial exfoliation, respectively, while the layered structure of Na^+MMT appeared to be intact at the 20% level indicating intercalation. Exfoliated structures have been observed previously at a low clay loading of 3% in starch/PVOH/Na^+MMT nanocomposites produced by melt processing.[31] A decreased degree of exfoliation/intercalation with increasing clay level has also been reported for polymer nanocomposites. In an earlier study, intercalation was observed at all levels of clay (3−21%) in starch/Na^+MMT nanocomposites produced by melt extrusion.[6] However, an increase in clay content beyond 6% appeared to result in a lower degree of exfoliation as inferred from a less steep decline in water vapor permeability of the films cast from the nanocomposites. In another study involving nanocomposite films prepared from cara-root starch, glycerol, and Ca^{2+} hectorite clay by solution casting, the degree of intercalation depended on

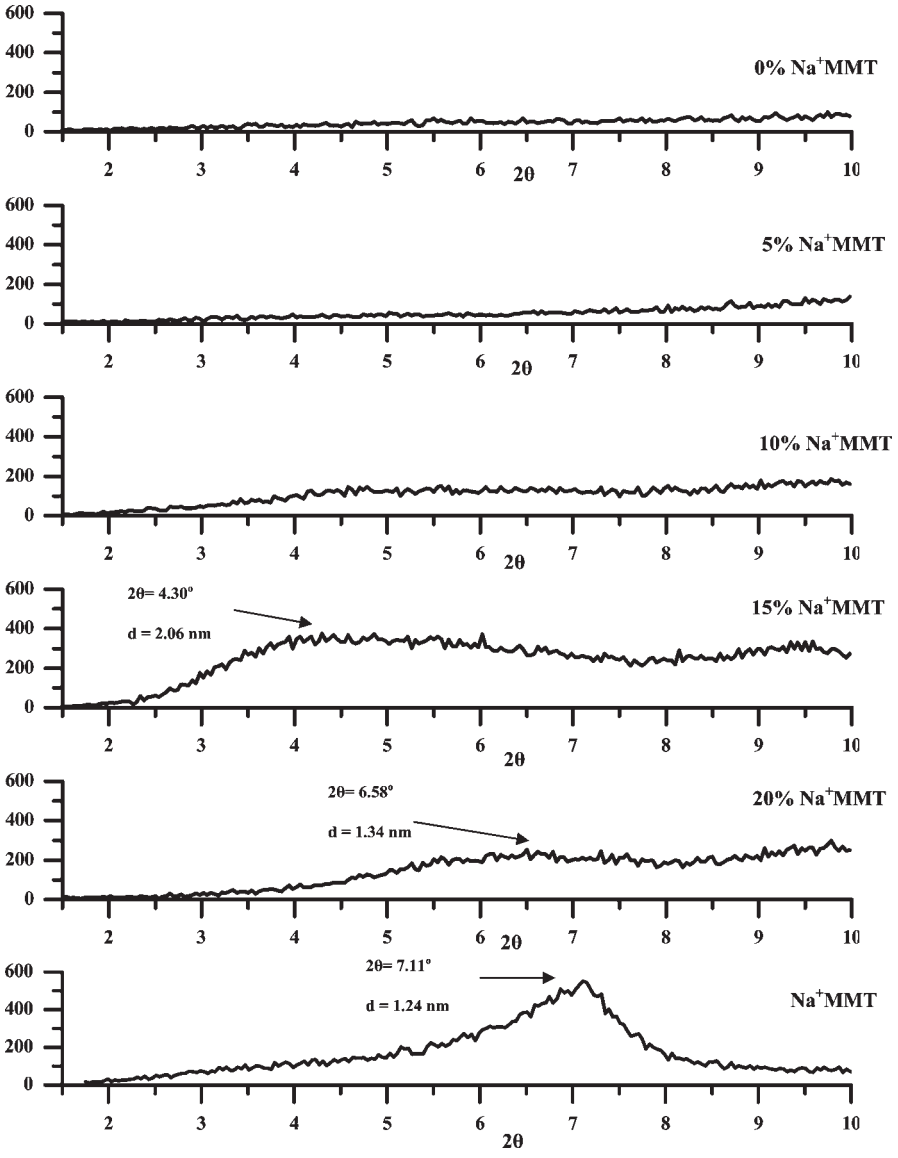

Figure 2. XRD patterns for pure Na^+MMT (bottom) and nanocomposites with 0−20% Na^+MMT.

the proportion of available clay and decreased with higher levels of clay.[34]

DSC analysis of nanocomposite films provided data on glass transition temperature (T_g) and change in heat capacity (ΔC_p) at T_g from which useful insight into structural conformations and interactions between polymers and clay could be inferred. T_g was determined as the midpoint of the glass transition region on the DSC scan. The T_g of the starch/PVOH composite with 0% Na^+MMT was 70.28 °C, while that of starch/PVOH/Na^+MMT nanocomposites with 5−20% Na^+MMT ranged from 71.75 to 61.22 °C (Table 2). In general, an increase in the Na^+MMT level from 5 to 20% led to a steady decrease in T_g, although the effect of Na^+MMT content on T_g was not statistically significant (p = 0.845). Conflicting effects of clay on polymer relaxation behavior, and thus the T_g of nanocomposites, have been reported depending on the interplay between the confinement of polymer chains, surface interactions, and disruption of the intermolecular structure.[24,35−39] In the current study where intercalated nanostructures were predominant, more polymer chains were likely to be confined between clay galleries as Na^+MMT content increased. This could result in the disruption of hydrogen bonding between OH groups within and across starch and PVOH chains. Thus, the stable intermolecular structure was disrupted, leading to a faster relaxation of chain segments and depressed T_g in the nanocomposites. A similar reasoning was offered for T_g depression with an increased 20AMMT clay level (2−10%) in amorphous polyamide (aPA) nanocomposites.[35] Change in heat capacity (ΔC_p) at the glass transition temperature gives information about the polymer chain mobility in nanocomposite systems as it depends on the internal degrees of freedom of molecular motion.[40] ΔC_p was significantly affected by the Na^+MMT level (p = 0.00118) and decreased from 0.05867 J/g·°C to 0.01751 J/g·°C as clay content increased from 0 to 20% (Table 2). This can also be attributed to increased polymer confinement at higher clay levels, which resulted in a decrease in the number of degrees of freedom for polymer chain segments.[35,40]

Data related to the physical properties of nanocomposite films are also summarized in Table 2. Na^+MMT content had a

significant effect on both tensile strength (p = 0.0001) and elongation at the break (p = 0.001). TS increased from 8.39 to 18.84 MPa and E% decreased from 136.82 to 41.57% as clay content increased from 0 to 20% (Table 2). This is consistent with several studies involving polymer−clay nanocomposite systems.[5,6,8,35,41,42] The clay−polymer interactions prevent easy sliding of the polymer chains against each other thus lowering elongation properties of the nanocomposites. However, higher clay content in an intercalated/exfoliated system leads to greater mechanical strength because the modulus of clay or the associated constrained region is several times higher than that of the polymer.[35] The mechanical properties of nanocomposites are determined not only by the modulus but also by the amount of constrained region. The latter depends on the degree of exfoliation/intercalation and the proximity of the polymer chains to the nanoclay layers. The constrained region clearly did not increase in the same proportion as the clay content, as inferred from TS data. This substantiated the earlier observation that the degree of intercalation reduced with an increase in the Na^+MMT level. Water vapor permeability was also significantly affected by Na^+MMT content (p = 0.001). WVP decreased from 1.68 to 0.718 g·mm/kPa·h·m^2 with an increase in Na^+MMT levels from 0 to 20% (Table 2). A similar trend was observed previously for starch/Na^+MMT nanocomposites.[6] Impermeable nanomaterials such as layered silicates decrease the permeability of gases not only by reducing the volume of material available for flow but also by creating more tortuous pathways.[6,43] However, in the absence of proper dispersion, formation of microvoids at the interface of the polymer and clay can compensate for the increase in tortuosity.[43] This might be the reason for the very little change in WVP between the 15 and 20% Na^+MMT loadings.

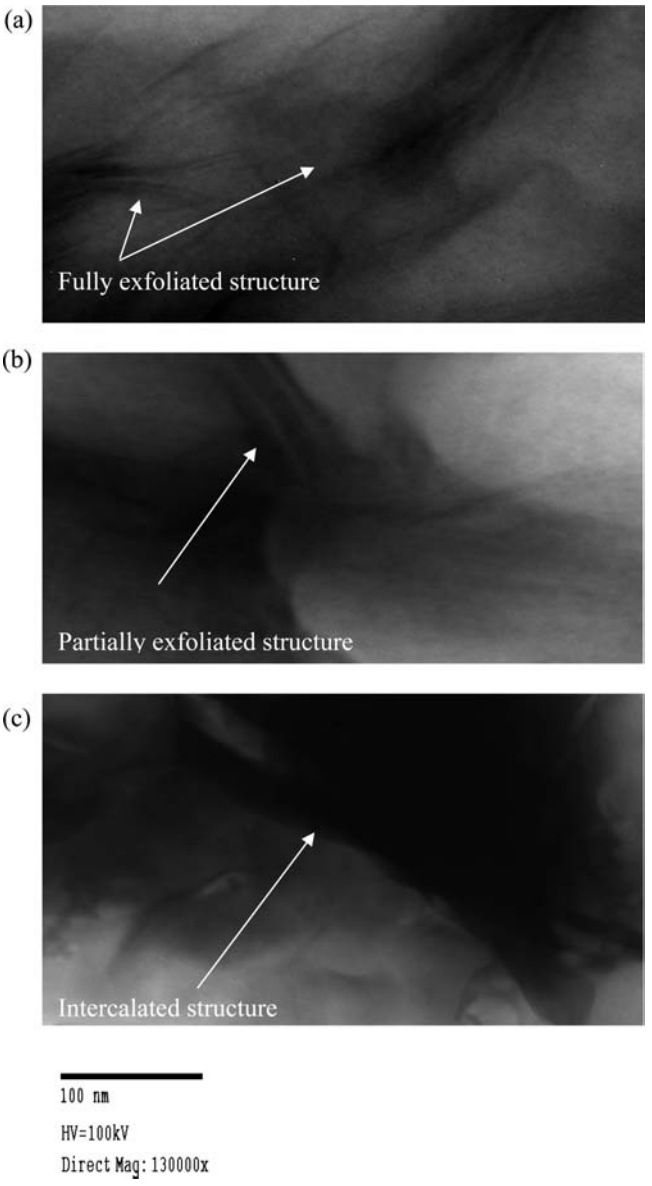

Figure 3. TEM scans for nanocomposites with (a) 5%, (b) 10%, and (c) 20% Na^+MMT.

PVOH Molecular Weight. XRD scans of starch/PVOH (1:1) composite films, with varying PVOH molecular weight and 10% Na^+MMT, are shown in Figure 4. Broader diffraction patterns with peaks at lower 2θ (3.53−4.15°) than natural Na^+MMT were observed in all cases, which indicated higher d-spacing and the formation of intercalated nanocomposites. The peak corresponding to lowest molecular weight PVOH (Celvol107) had an intensity of ∼150, which was much lower than that for other PVOH types (∼280−400). The low peak intensity for Celvol107 indicated that some silicate layers were disrupted resulting in partial exfoliation, whereas other nanocomposites had intercalated structures with a broad range of d-spacing between clay platelets. During the solution mixing process, hydration of Na^+ ions causes MMT to swell, which results in increased d-spacing. This phenomenon greatly helps the starch and PVOH polymers to enter silicate galleries to form intercalated nanocomposites.[23] Temperature or heat plays an important role in intercalation and exfoliation in such systems by increasing the mobility of the polymers. Heat also causes degradation of starch that assists in mobility. In addition, glycerol makes hydrogen bonds with the polymers and creates a plasticization effect, which further increases polymer mobility. However, higher molecular weight implies greater size and reduced mobility of the polymers,[44−47] which makes it difficult for PVOH to penetrate the interlayer galleries of Na^+MMT and results in intercalated nanostructures but the absence of exfoliation in the case of Celvol310, Celvol325, and Celvol350.

PVOH molecular weight had a significant effect on T_g of nanocomposite films (p = 0.01043). T_g was 65.14, 71.0, 74.94,

Table 2. Thermal and Physical Properties of Nanocomposite Films with Different Na^+MMT Contents

Na^+MMT (%)	T_g (°C)	ΔC_p (J/g·°C)	TS (MPa)	E%	WVP (g·mm/kPa·h·m^2)
0	70.28 ± 13.27	0.0587 ± 0.0099	8.39 ± 0.59	136.82 ± 11.82	1.6828 ± 0.057
5	71.75 ± 12.38	0.0404 ± 0.0112	11.60 ± 0.62	103.00 ± 17.03	1.2353 ± 0.099
10	68.45 ± 12.03	0.0390 ± 0.0108	17.06 ± 1.86	101.28 ± 13.14	1.0537 ± 0.050
15	66.14 ± 10.19	0.0230 ± 0.0031	18.84 ± 1.27	61.83 ± 6.99	0.7255 ± 0.023
20	61.22 ± 8.53	0.0175 ± 0.0366	18.41 ± 0.91	41.57 ± 3.77	0.7185 ± 0.230

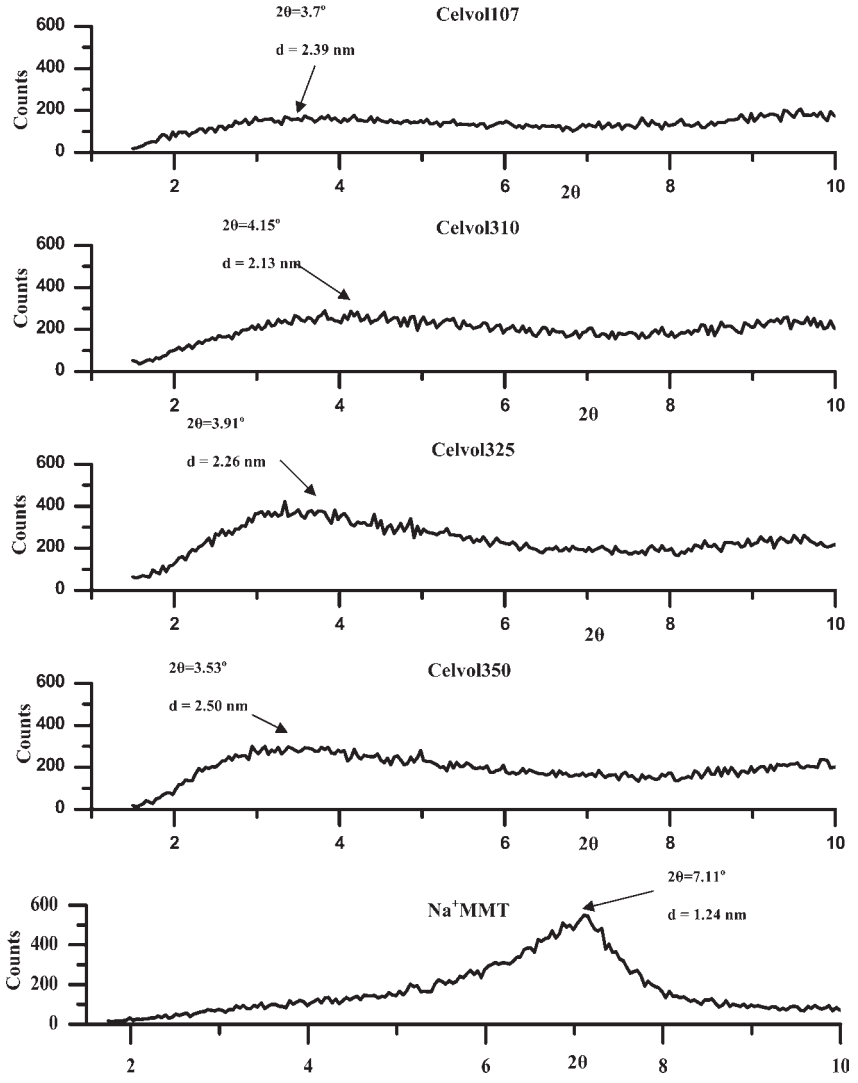

Figure 4. XRD patterns for pure Na^+MMT (bottom) and nanocomposites containing different types of PVOH. Higher Celvol numbers correspond to a greater molecular weight.

Table 3. Thermal and Physical Properties of Nanocomposite Films with Different PVOH Molecular Weights[a]

PVOH type	T_g (°C)	ΔC_p (J/g·°C)	T_m (°C)	TS (MPa)	E%	WVP (g·mm/kPa·h·m^2)
Celvol107	63.55 ± 0.045	0.045 ± 0.0046	162.49 ± 3.08	11.87 ± 0.48	66.73 ± 13.17	1.411 ± 0.105
Celvol310	66.44 ± 0.047	0.048 ± 0.0130	159.52 ± 3.13	13.46 ± 1.06	80.58 ± 13.32	1.295 ± 0.066
Celvol325	73.60 ± 0.064	0.064 ± 0.0150	159.40 ± 5.35	16.44 ± 0.85	161.85 ± 8.99	1.165 ± 0.084
Celvol350	72.60 ± 0.064	0.068 ± 0.0356	159.04 ± 5.00	14.38 ± 0.49	162.20 ± 26.95	1.293 ± 0.024

[a] Higher Celvol numbers correspond to agreater molecular weight.

and 72.60 °C, respectively, for nanocomposites containing Celvol107, Celvol310, Celvol325, and Celvol350 (Table 3). The increase in T_g of starch/PVOH/Na^+MMT nanocomposites followed by a plateau appeared to be a function of bulk polymer molecular weight rather than any nanoscale effect. It is well-known that T_g of polymers increases with increasing molecular weight.[35,48,49] Smaller polymers have a greater number of chain end segments in a given weight of polymer and therefore increased segmental movement.[49] T_g increases with higher molecular weight because segmental motion gets restricted in larger polymers. This increase in glass transition temperature continues until the molecular weight reaches a critical level beyond which T_g reaches an asymptotic value.[35] PVOH molecular weight did not have a significant impact on ΔC_p ($p = 0.482$), although the latter increased from 0.0454 to 0.0676 J/g·°C with increasing molecular weight of PVOH (Table 3). Larger ΔC_p indicated a greater number of internal degrees of freedom, possibly due to reduced interactions between higher molecular weight PVOH and Na^+MMT. Peak melting temperatures (T_m) were also not affected significantly by PVOH molecular weight ($p = 0.7437$). T_m of nanocomposites ranged from 159.04 to 162.49 °C, with only small differences between PVOH types

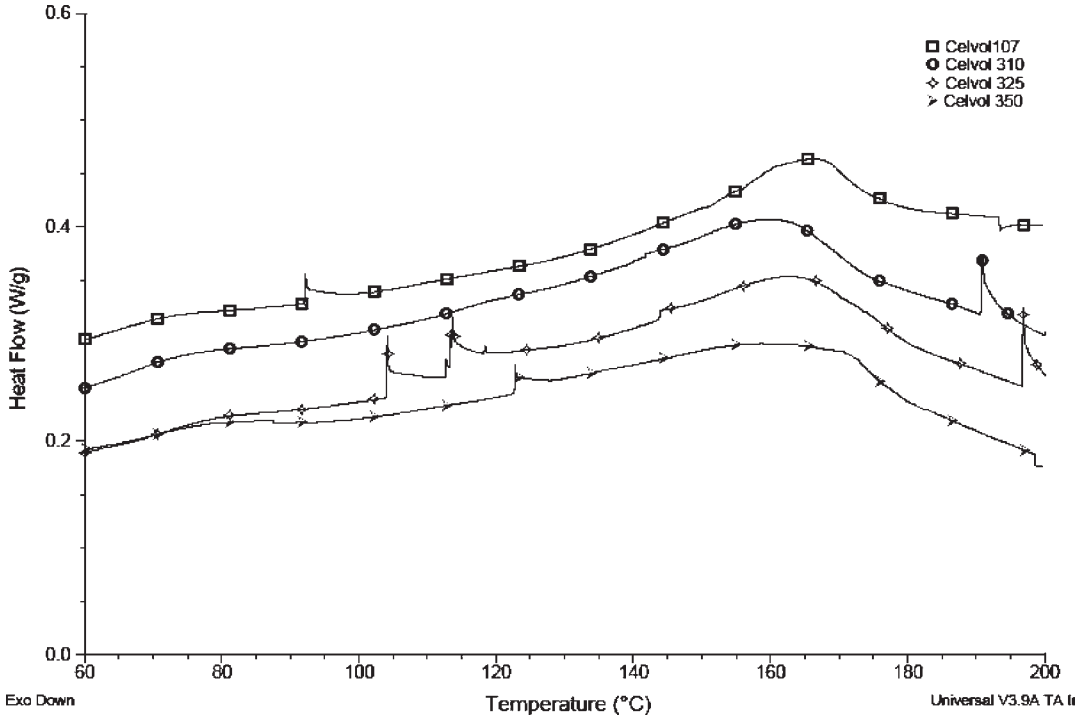

Figure 5. DSC scans showing melting peaks for nanocomposites with different PVOH molecular weights. Higher Celvol numbers correspond to a greater molecular weight.

(Table 3). This was expected as all four PVOH types used in this study were fully hydrolyzed resulting in the same melting temperature range. However, DSC scans exhibited broadening of the melting peak for nanocomposites with increasing molecular weight of PVOH (Figure 5). A broader melting range with increasing molecular weight could be due to increased interactions between starch and PVOH molecules. As the PVOH chain length increased with higher molecular weight, it was harder for these chains to enter the silicate interlayer galleries as described earlier. This reduced interactions between PVOH and Na^+MMT but increased the opportunity for hydrogen bonding between the hydroxyl groups of starch and PVOH. Molecular interactions among starch, PVOH, and Na^+MMT are described in greater detail later.

Physical properties of nanocomposite films from different molecular weight PVOH are summarized in Table 3. While the mechanical strength and barrier properties of nanocomposite films are affected by the degree of intercalation and exfoliation in the system, it was clear that the impact of PVOH molecular weight was mainly determined by physical properties of the matrix and not any nanoscale effects. Both tensile strength and E% were significantly affected by PVOH molecular weight (p = 0.000559 and 0.000149, respectively). Tensile strength for nanocomposites with Celvol107, Clevol310, and Celvol325 was 11.87, 13.84, and 16.44 MPa, respectively, but this increasing trend was discontinued with a decrease to 14.38 MPa for Celvol350. The increase in tensile strength was primarily due to bulk polymer molecular weight rather than interactions with Na^+MMT.[50] Increasing molecular weight leads to greater physical entanglement of polymer chains.[3] The entanglement effect, however, tapers off at very high molecular weight. A previous study involving 1:1 blends of *Amaranthus cruentus* flour with PVOH of varying molecular weights also reported a significant increase in tensile strength of composites having Celvol325 as compared to Celvol107.[51] No significant difference was reported in tensile strength of composites having Celvol325 and Celvol350. For pure PVOH based films, however, decreased tensile strength with increasing molecular weight has been observed.[52] This decrease was attributed to the reduction in crystallinity of the polymer with increasing molecular weight. No information was provided on the degree of hydrolysis of PVOH, which can have a significant impact on mechanical strength.[50] In any case, the entanglement effect with higher molecular weight appears to predominate for composite films involving starch-based materials and PVOH. At molecular weights higher than Celvol325, reduced crystallinity could have a role in decreasing the tensile strength of starch/PVOH/Na^+MMT nanocomposites. E% also increased from 66.73% to 161.85% as PVOH molecular weight increased (Celvol107 to Celvol325) and appeared to plateau with a further increase in molecular weight (Celvol 350). Similar trends were reported previously for composites of PVOH with amaranthus flour[51] and nanocomposites involving nylon-6 and organically modified MMT.[53] Polymer chain length is an important factor in determining the elongation at the break.[3] Higher molecular weight PVOH polymer chains are longer and can easily slide past each other while forming new hydrogen bonds with adjacent polymer chains, thus leading to greater ductility. The lower polymer/Na^+MMT interactions with increased molecular weight could have further reinforced this effect.

PVOH molecular weight also had a significant effect on water vapor permeability of nanocomposite films (p = 0.02732). As molecular weight increased up to Celvol325, WVP decreased from 1.41 to 1.16 g·mm/kPa·h·m^2 (Table 3). A nonsignificant increase in WVP to 1.29 g·mm/kPa·h·m^2 was observed with a further increase in molecular weight (Celvol350). From a

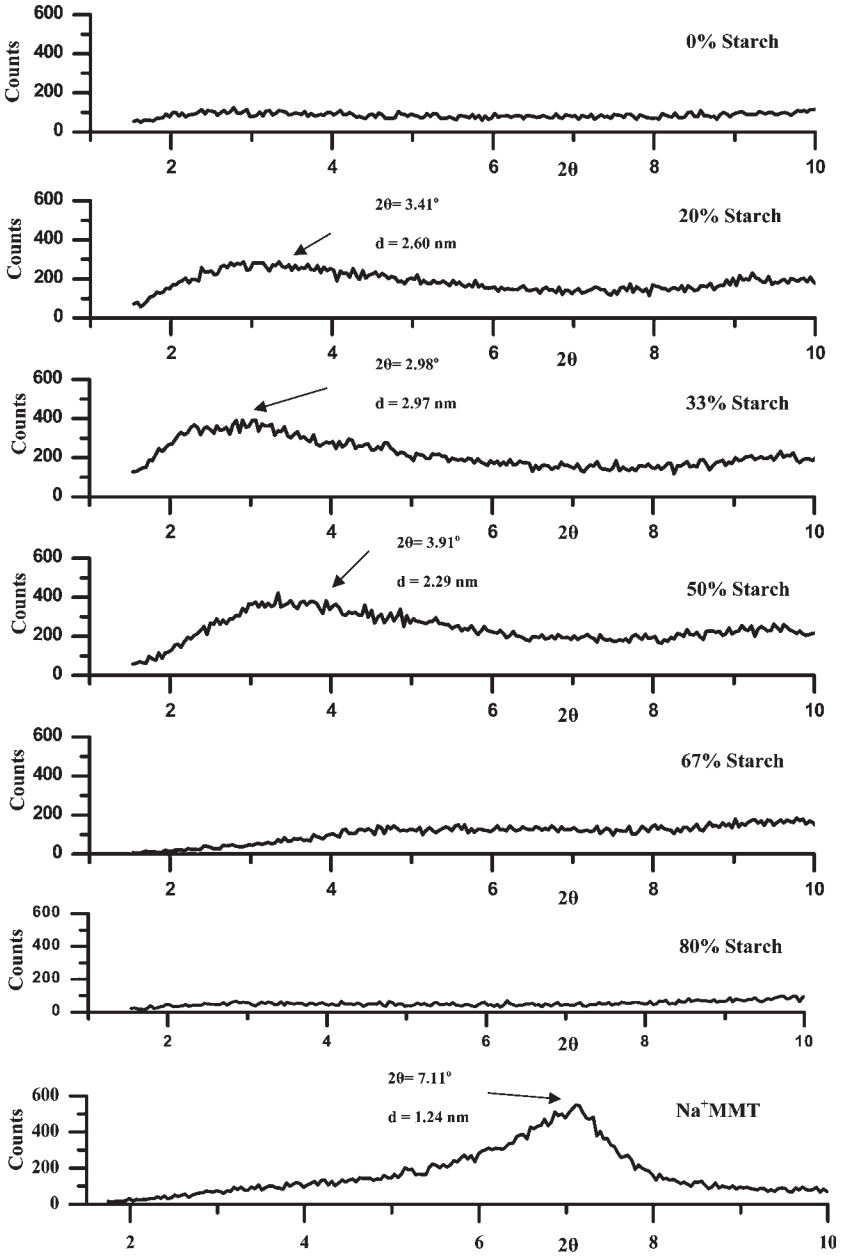

Figure 6. XRD patterns for pure Na^+MMT (bottom) and nanocomposites with different starch contents.

fundamental point of view, the permeability of any gas depends on the solubility and diffusion coefficient with respect to the medium as described through the following relationship:

$$P = D \times S \quad (6)$$

where P = gas permeability, D = diffusion coefficient, and S = solubility coefficient. The water resistance of Celvol polymers increases at higher molecular weight.[50] Moreover, the diffusion coefficient of any gas typically reduces with an increase in polymer viscosity. The combination of these factors was responsible for the decrease in WVP with increasing PVOH molecular weight. The departure from this trend in the case of Celvol350 can be attributed to higher molecular weight leading to the reduced dispersion of Na^+MMT in the polymer matrix and also lower crystallinity.[51]

Starch Content. X-ray diffraction scans of starch/PVOH composite films with varying levels of starch and 10% Na^+MMT are shown in Figure 6. No XRD peaks were detected at starch levels of 0, 67, and 80%. This indicated the formation of fully exfoliated nanocomposite structures. Films with 20−50% starch had intensity peaks, but they corresponded to lower 2θ (2.98−3.91°) and higher d-spacing (2.29−2.97 nm) than those of natural Na^+MMT (2θ of 7.11° and d-spacing of 1.24 nm). This indicated the formation of intercalated nanocomposites. The XRD peaks were also broader than the pure Na^+MMT peak, which was evidence for partial exfoliation.

Starch content did not have a significant effect on T_g (p = 0.2095). However, an increase in T_g from 71.49 to 76.95 °C was observed as the starch level increased from 0 to 33%, which was followed by a monotonic decrease to 67.03 °C as the starch level increased to 80% (Table 4). The initial increase in T_g can be

Table 4. Thermal and Physical Properties of Nanocomposite Films with Different Starch Contents

starch (%)	moisture (%)	T_g (°C)	ΔC_p (J/g·°C)	T_m (°C)	TS (MPa)	E%	WVP (g·mm/kPa·h·m^2)
0	16.4 ± 0.7	71.49 ± 1.70	0.03495 ± 0.0139	164.00 ± 6.25	23.01 ± 1.30	291.28 ± 57.34	1.483 ± 0.116
20	13.8 ± 0.5	74.01 ± 2.87	0.08276 ± 0.0176	162.13 ± 1.00	22.35 ± 1.93	211.40 ± 28.44	1.430 ± 0.040
33	13.6 ± 0.6	76.95 ± 8.30	0.05671 ± 0.0078	159.76 ± 1.88	18.21 ± 3.06	187.49 ± 11.52	1.247 ± 0.120
50	10.4 ± 0.8	73.60 ± 3.39	0.06406 ± 0.0156	159.53 ± 4.68	16.44 ± 0.85	161.85 ± 8.99	1.165 ± 0.084
67	12.0 ± 0.7	68.34 ± 4.00	0.03899 ± 0.0108	156.54 ± 5.22	17.06 ± 0.87	101.28 ± 13.14	1.054 ± 0.050
80	14.9 ± 1.5	67.03 ± 4.26	0.01615 ± 0.0125	156.31 ± 3.38	18.08 ± 0.88	28.93 ± 9.82	1.048 ± 0.069

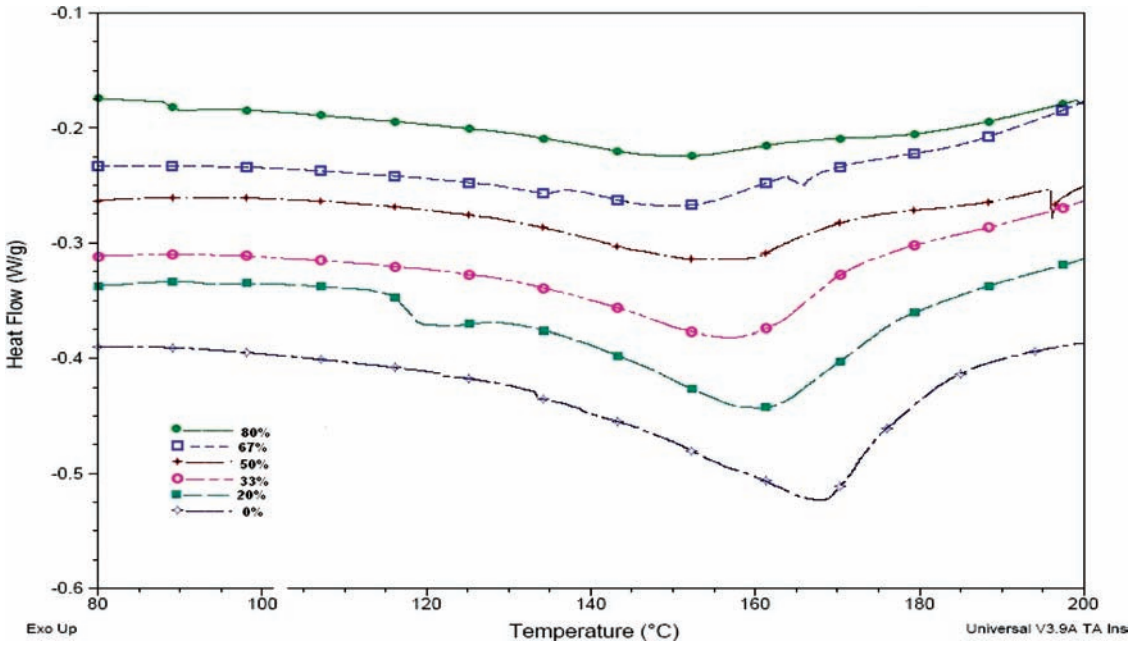

Figure 7. DSC scans showing melting peaks for nanocomposites with different starch contents.

attributed to strong interactions between starch and PVOH that resulted in the restricted segmental movement of polymer chains. As starch content increased beyond 33%, the lower T_g of starch as compared to that of PVOH had a predominant role in depressing the overall T_g of the nanocomposites. Moisture content of the nanocomposite films might also have a role in determining T_g, as water is a plasticizer for both starch and PVOH. Equilibrium moisture decreased from 16.42 to 10.43% as the starch level increased from 0 to 50% (Table 4), probably due to hydrogen bonding between starch and PVOH and the reduced affinity to water. Moisture increased to 14.88% with a further increase in the starch level due to lesser hydroxyl groups involved in starch−PVOH interactions. The extent of intercalation/exfoliation might be another factor that impacted the T_g, but the interactions between starch and PVOH appeared to predominate. This was further confirmed by the change in the specific heat at T_g (Table 4). Starch content had a significant effect on ΔC_p (p = 0.0008). Higher ΔC_p was observed for nanocomposites with 20−50% starch as compared to those of other starch levels, indicating lower internal degrees of freedom due to the increased interaction between polymers.

Starch content did not have a significant effect on melting temperature (p = 0.4110), although a gradual decrease in T_m from 164.00 to 156.31 °C was observed as starch increased from 0 to 80% (Table 4). DSC scans also showed broadening in melting temperature peaks with increasing starch level (Figure 7). This broadening can be attributed to increased hydrogen bonding between starch and PVOH. A slight decrease in T_m of starch/PVOH extruded blends with increasing starch content, accompanied by broadening of the melting peaks, was also observed in a previous study.[16] Decrease in PVOH crystallinity and restraining of PVOH molecules by starch were mentioned as the contributing factors.

XRD and DSC results discussed above provided a good understanding of polymer/polymer and polymer/clay interactions in starch/PVOH/Na^+MMT nanocomposites and the relative intensity of these interactions. Apart from intramolecular bonding, three types of interactions take place at the molecular level in this multicomponent system (Figure 8): (i) hydrogen bonding between hydroxyl groups of starch and PVOH, (ii) interactions between PVOH hydroxyl groups and Na^+ ions of Na^+MMT, and (iii) interactions between hydroxyl groups of starch and Na^+ ions of Na^+MMT. Consistent with the high miscibility of starch/PVOH,[16,19] the interactions between the two polymers appeared to be the strongest and were followed by starch/Na^+MMT and PVOH/Na^+MMT interactions. On the basis of this insight, a conceptual model was developed for changes in intensity of PVOH/Na^+MMT and starch/Na^+MMT interactions at different starch contents (Figure 9). In the absence of starch, interactions of PVOH with Na^+MMT were

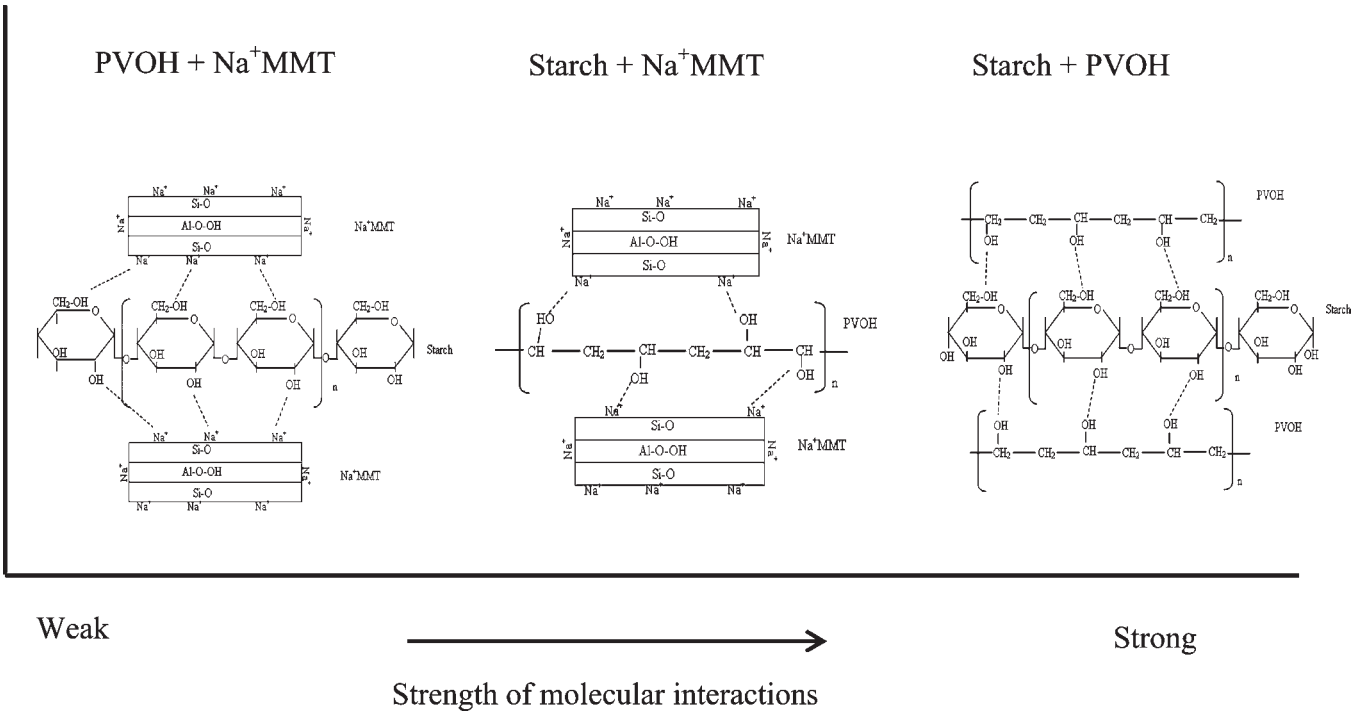

Figure 8. Molecular interaction between various components of the nanocomposite system and their relative strengths.

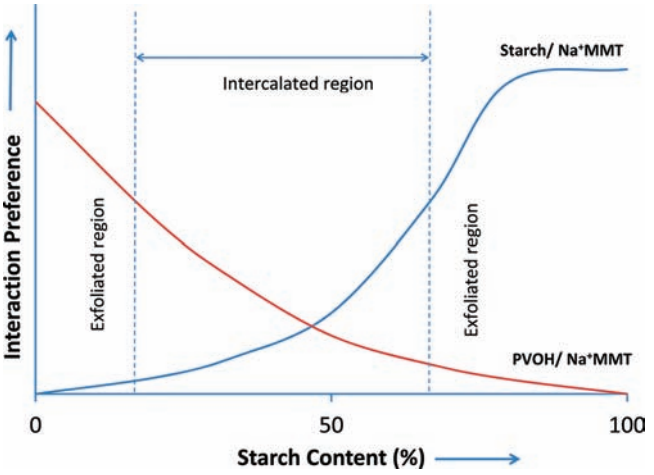

Figure 9. Conceptual model for PVOH/Na^+MMT and starch/Na^+MMT interactions at different starch contents.

strong enough to rupture the layered silicate structure and form exfoliated nanocomposites. With the addition of starch, stronger hydrogen bonds were formed between the two polymers that reduced the intensity of PVOH/Na^+MMT intercations and also increased the effective polymer chain lengths. This decreased exfoliation and resulted in intercalated nanocomposites. As starch content increased to 67 and 80%, there were sufficient numbers of hydroxyl groups in the system available to interact with Na^+MMT that lead again to the formation of exfoliated nanostructures.

Tensile strength and elongation at the break data for nanocomposite films with varying starch contents are shown in Table 4. The starch level had a significant effect on both TS ($p = 0.0004$) and E% ($p = 0.0001$). TS decreased from 23.01 to 16.44 MPa with an increase in starch content from 0 to 50%, followed by a gradual increase up to 18.08 MPa as starch increased to 80%. E% continuously decreased from 291.28 to 28.93% with an increase in starch content from 0 to 80%. A decrease in tensile strength and elongation at the break with higher starch content in starch/PVOH blends has been observed previously.[14,15,19,22] The strength of covalent bonding between monomeric units and the length and flexibility of polymer chains impact these mechanical properties. Starch has inferior tensile strength and elongation properties than PVOH,[14] which was the primary reason for the deterioration in mechanical performance as the proportion of starch increased in starch/PVOH/Na^+MMT nanocomposite films. The observed departure from this trend, in the form of an increase in TS at the starch contents of 67 and 80%, could be due to the formation of exfoliated nanocomposites as discussed above. Water vapor permeability of the nanocomposite films was also significantly affected by starch content ($p = 0.0001$). WVP decreased monotonically from 1.483 to 1.048 g·mm/kPa·h·m^2 with an increase in starch content from 0 to 80% (Table 4). Less affinity to water due to hydrogen bonding between starch and PVOH might be one reason, although conflicting results have been reported previously for starch/PVOH blends.[16,22,51] The intercalated and exfoliated nanostructures in the current study were also an important factor that impacted permeability.

In summary, utilization of PVOH in multi-component nanocomposites led to a significant enhancement in mechanical properties, especially elongation at the break, as compared to those of starch/Na^+MMT nanocomposites studied previously.[6,7] Relative to composites of starch/PVOH devoid of any nano fillers,[14−16,22] the starch/PVOH/Na^+MMT nanocomposites had improved tensile strength and comparable or better elongation properties. Also the content of the cheaper and renewable component, i.e., starch, could be enhanced up to 50%, while

maintaining mechanical properties comparable to plastic-based packaging films.[9] This has significant implications for nonpetroleum, green, biodegradable packaging. Water vapor permeability of starch/PVOH/Na^+MMT nanocomposite films was comparable to that of starch/Na^+MMT nanocomposite films as reported previously[6] but was much lower than plastic films.[10] It is clear that research needs to be focused in this direction, especially with regard to high-performance nano fillers and the improvement of matrix properties by methods such as cross-linking. Also, scalable technologies, such as melt extrusion, need to be developed for production of the nanocomposites.

AUTHOR INFORMATION

Corresponding Author

*Tel: +1 785 532 2403. Fax: +1 785 532 4017. E-mail: salavi@ksu.edu.

Funding Sources

The project was supported by the National Research Initiative Competitive Grants Program of the United States Department of Agriculture, grant number 20081503. This is contribution number 10-299-J from the Kansas Agricultural Experiment Station, Manhattan, KS, 66506.

REFERENCES

(1) Marsh, K.; Bugusu, B. Food packaging: roles, materials, and environmental issues. *J. Food Sci.* **2007**, *72*, R39–R55.

(2) Robertson, G. L. *Food Packaging: Principles and Practice*, 2nd ed.; CRC Press: Boca Raton, FL, 2006; pp 1−42.

(3) Nielsen, L. E.; Landel, R. F. *Mechanical Properties of Polymers and Composites*, 2nd ed.; Marcel Dekker, Inc.: New York, 1994; pp 1−32.

(4) Tang, X. Z.; Kumar, P.; Alavi, S.; Sandeep, K. P. Recent advances in biopolymer-based food packaging materials. *Crit. Rev. Food Sci. Nutr.* **2011**, DOI: 10.1080/10408398.2010.500508.

(5) Dean, K. M.; Do, M. D.; Petinakis, E.; Yu, L. Key interactions in biodegradable thermoplastic starch/poly(vinyl alcohol)/montmorillonite micro- and nanocomposites. *Compos. Sci. Technol.* **2008**, *68*, 1453–1462.

(6) Tang, X.; Alavi, S.; Herald, T. J. Barrier and mechanical properties of starch-clay nanocomposite films. *Cereal Chem.* **2008**, *85*, 433–439.

(7) Tang, X.; Alavi, S.; Herald, T. J. Effects of plasticizers on the structure and properties of starch-clay nanocomposite films. *Carbohydr. Polym.* **2008**, *74*, 552–558.

(8) Dean, K.; Yu, L.; Wu, D. Y. Preparation and characterization of melt-extruded thermoplastic starch/clay nanocomposites. *Compos. Sci. Technol.* **2007**, *67*, 413–421.

(9) van Krevelen, D. W.; te Nijenhuis, K. *Properties of Polymers: Their Correlation with Chemical Structure; Their Numerical Estimation and Prediction from Additive Group Contributions*, 2nd ed.; Elsevier: Amsterdam, The Netherlands, 2009; pp 889−956.

(10) Massey, L. K. *Permeability Properties of Plastics and Elastomers: A Guide to Packaging and Barrier Materials*, 2nd ed.; William Andrew Publishing: Norwich, NY, 2003; pp 209−292.

(11) Parulekar, Y.; Mohanty, A. K. Extruded biodegradable cast films from polyhydroxyalkanoate and thermoplastic starch blends: fabrication and characterization. *Macromol. Mater. Eng.* **2007**, *292*, 1218–1228.

(12) Jun, C. L. Reactive blending of biodegradable polymers: PLA and starch. *J. Polym. Environ.* **2000**, *8*, 33–37.

(13) Jang, W. Y.; Shin, B. Y.; Lee, T. J.; Narayan, R. Thermal properties and morphology of biodegradable PLA/starch compatibilized blends. *J. Ind. Eng. Chem.* **2007**, *13*, 457–464.

(14) Mao, L. J.; Imam, S.; Gordon, S.; Cinelli, P.; Chiellini, E. Extruded cornstarch-glycerol-polyvinyl alcohol blends: mechanical properties, morphology, and biodegradability. *J. Polym. Environ.* **2000**, *8*, 205–211.

(15) Yang, S.-Y.; Huang, C.-Y. Plasma treatment for enhancing mechanical and thermal properties of biodegradable PVA/starch blends. *J. Appl. Polym. Sci.* **2008**, *109*, 2452–2459.

(16) Zou, G.-X.; Ping-Qu, J.; Liang-Zou, X. Extruded starch/PVA composites: water resistance, thermal properties, and morphology. *J. Elastomers Plast.* **2008**, *40*, 303–316.

(17) Follain, N.; Joly, C.; Dole, P.; Bliard, C. Properties of starch based blends. Part 2. Influence of poly vinyl alcohol addition and photocrosslinking on starch based materials mechanical properties. *Carbohydr. Polym.* **2005**, *60*, 185–192.

(18) Marten, F. L.; Zvanut, C. W. Hydrolysis of Polyvinyl Alcohol to Polyvinyl Acetate. In *Polyvinyl Alcohol: Developments*, 2nd ed.; Finch, C. A., Ed.; John Wiley & Sons Ltd: Chichester, England, 1992; pp 57−76.

(19) Tang, X.; Alavi, S. Recent advances in starch, polyvinyl alcohol based polymer blends, nanocomposites and their biodegradability. *Carbohydr. Polym.* **2011**, *85*, 7–16.

(20) Zhou, X. Y.; Cui, Y. F.; Jia, D. M.; Xie, D. Effect of a complex plasticizer on the structure and properties of the thermoplastic PVA/starch blends. *Polym.-Plast. Technol. Eng.* **2009**, *48*, 489–495.

(21) Russo, M. A. L.; O'Sullivan, C.; Rounsefell, B.; Halley, P. J.; Truss, R.; Clarke, W. P. The anaerobic degradability of thermoplastic starch: polyvinyl alcohol blends: potential biodegradable food packaging materials. *Bioresour. Technol.* **2009**, *100*, 1705–1710.

(22) Ramaraj, B. Crosslinked poly(vinyl alcohol) and starch composite films: study of their physicomechanical, thermal, and swelling properties. *J. Appl. Polym. Sci.* **2007**, *103*, 1127–1132.

(23) Paul, D. R.; Robeson, L. M. Polymer nanotechnology: nanocomposites. *Polymer* **2008**, *49*, 3187–3204.

(24) Chen, B.; Evans, J. R. G.; Greenwell, H. C.; Boulet, P.; Coveney, P. V.; Bowden, A. A.; Whiting, A. A critical appraisal of polymer-clay nanocomposites. *Chem. Soc. Rev.* **2008**, *37*, 568–594.

(25) Alexandre, M.; Dubois, P. Polymer-layered silicate nanocomposites: preparation, properties and uses of a new class of materials. *Mater. Sci. Eng., R* **2000**, *28*, 1–63.

(26) Tang, X.; Alavi, S. Development and Characterization of Starch Based Nano-Composites. In *Handbook of Carbohydrate Polymers: Development, Properties and Applications*; Ito, R., Matsuo, Y., Eds.; Nova Science Publishers, Inc.: Hauppauge NY, 2010; pp 45−83.

(27) Avella, M.; De Vlieger, J. J.; Errico, M. E.; Fischer, S.; Vacca, P.; Volpe, M. G. Biodegradable starch/clay nanocomposite films for food packaging applications. *Food Chem.* **2005**, *93*, 467–474.

(28) Strawhecker, K. E.; Manias, E. Structure and properties of poly(vinyl alcohol)/Na+ montmorillonite nanocomposites. *Chem. Mater.* **2000**, *12*, 2943–2949.

(29) Lim, L. Y.; Wan, L. S. C. The effect of plasticizers on the properties of polyvinyl alcohol films. *Drug Dev. Ind. Pharm.* **1994**, *20*, 1007–1020.

(30) Spiridon, I.; Popescu, M. C.; Bodarlau, R.; Vasile, C. Enzymatic degradation of some nanocomposites of poly(vinyl alcohol) with starch. *Polym. Degrad. Stab.* **2008**, *93*, 1884–1890.

(31) Dimonie, D.; Constantin, R.; Vasilievici, G.; Popescu, M. C.; Garea, S. The dependence of the XRD morphology of some bionanocomposites on the silicate treatment. *J. Nanomater.* **2008**, DOI:10.1155/2008/538421.

(32) Vasile, C.; Stoleriu, A.; Popescu, M.-C.; Duncianu, C.; Kelnar, I.; Dimonie, D. Morphology and thermal properties of some green starch/poly(vinyl alcohol)/montmorillonite nanocomposites. *Cellul. Chem. Technol.* **2008**, *42*, 549–568.

(33) Ahmad, M. B.; Shameli, K.; Darroudi, M.; Yunus, W. M. Z. W.; Ibrahim, N. A. Synthesis and characterization of silver/clay/chitosan bionanocomposites by UV-irradiation method. *Am. J. Appl. Sci.* **2009**, *6*, 2030–2035.

(34) Wilhelm, H.-M.; Sierakowski, M.-R.; Souza, G. P.; Wypych, F. Starch films reinforced with mineral clay. *Carbohydr. Polym.* **2003**, *52*, 101–110.

(35) Zhang, X.; Loo, L. S. Study of glass transition and reinforcement mechanism in polymer/layered silicate nanocomposites. *Macromolecules* **2009**, *42*, 5196–5207.

(36) Lu, H.; Nutt, S. Restricted relaxation in polymer nanocomposites near the glass transition. *Macromolecules* **2003**, *36*, 4010–4016.

(37) Tran, T. A.; Said, S.; Grohens, Y. Nanoscale characteristic length at the glass transition in confined syndiotactic poly(methyl methacrylate). *Macromolecules* **2005**, *38*, 3867–3871.

(38) Vaia, R. A.; Sauer, B. B.; Tse, O. K.; Giannelis, E. P. Relaxations of confined chains in polymer nanocomposites: glass transition properties of poly(ethylene oxide) intercalated in montmorillonite. *J. Polym. Sci., Part B: Polym. Phys.* **1997**, *35*, 59–67.

(39) Zax, D. B.; Yang, D.-K.; Santos, R. A.; Hegemann, H.; Giannelis, E. P.; Manias, E. Dynamical heterogeneity in nanoconfined poly(styrene) chains. *J. Chem. Phys.* **2000**, *112*, 2945–2951.

(40) Vyazovkin, S.; Dranca, I. A DSC study of α and β-relaxations in a PS-clay system. *J. Phys. Chem. B* **2004**, *108*, 11981–11987.

(41) Chivrac, F.; Pollett, E.; Schmutz, M.; Averous, L. New approach to elaborate exfoliated starch-based nanobiocomposites. *Biomacromolecules* **2008**, *9*, 896–900.

(42) Ray, S. S.; Okamoto, M. Polymer/layered silicate nanocomposites: a review from preparation to processing. *Prog. Polym. Sci.* **2003**, *28*, 1539–1641.

(43) Sorrentino, A.; Tortora, M.; Vittoria, V. Diffusion behavior in polymer-clay nanocomposites. *J. Polym. Sci., Part B: Polym. Phys.* **2006**, *44*, 265–274.

(44) Zhong, Y.; De Kee, D. Morphology and properties of layered silicate-polyethylene nanocomposite blown films. *Polym. Eng. Sci.* **2005**, *45*, 469–477.

(45) Vaia, R. A.; Jandt, K. D.; Kramer, E. J.; Giannelis, E. P. Kinetics of polymer melt intercalation. *Macromolecules* **1995**, *28*, 8080–8085.

(46) Shen, Z.; Simon, G. P.; Cheng, Y.-B. Effects of molecular weight and clay organo-ions on the melt intercalation of poly(ethylene oxide) into layered silicates. *Polym. Eng. Sci.* **2002**, *42*, 2369–2382.

(47) Lee, E. C.; Mielewski, D. F.; Baird, R. J. Exfoliation and dispersion enhancement in polypropylene nanocomposites by in-situ melt phase ultrasonication. *Polym. Eng. Sci.* **2004**, *44*, 1773–1782.

(48) Ngai, K. L. The Glass Transition and the Glassy State. In *Physical Properties of Polymers*, 3rd ed.; Mark, J., Ngai, K., Graessley, W., Mandelkem, L., Samulski, E., Koenig, J., Wignall, G., Eds.; Cambridge University Press: Cambridge, U.K., 2004; pp 72−152.

(49) Gowariker, V. R; Viswanathan, N. V; Sreedhar, J. *Polymer Science*, 1st ed.; New Age International (P) Ltd.: New Delhi, India, 1986; pp 150−172.

(50) Sekisui Specialty Chemicals America. Typical properties of Celvol polyvinyl alcohol. http://www.sekisui-sc.com/sekisui/pvoh_products_properties.htm (accessed Aug 14, 2010).

(51) Elizondo, N. J.; Sobral, P. J. A.; Menegalli, F. C. Development of films based on blends of *Amaranthus cruentus* flour and poly(vinyl alcohol). *Carbohydr. Polym.* **2009**, *75*, 592–598.

(52) Abd El-Kader, K. A. M.; Abdel Hamied, S. F.; Mansour, A. B.; El-Lawindy, A. M. Y.; El-Tantaway, F. Effect of the molecular weights on the optical and mechanical properties of poly(vinyl alcohol) films. *Polym. Test.* **2002**, *21*, 847–850.

(53) Fornes, T. D.; Yoon, P. J.; Keskkula, H.; Paul, D. R. Nylon 6 nanocomposites: the effect of matrix molecular weight. *Polymer* **2001**, *42*, 9929–9940.